American Journal of Ophthalmology Case Reports 28 (2022) 101741

Contents lists available at ScienceDirect

American Journal of Ophthalmology Case Reports

journal homepage: www.ajocasereports.com/

Autofluorescent hyperreflective foci on infrared autofluorescence adaptive optics ophthalmoscopy in central serous chorioretinopathy

Kari V. Vienola [a,*], Raphael Lejoyeux [a,b], Elena Gofas-Salas [a], Valerie C. Snyder [a], Min Zhang [a], Kunal K. Dansingani [a], José-Alain Sahel [a], Jay Chhablani [a], Ethan A. Rossi [a,c,d]

[a] University of Pittsburgh, Department of Ophthalmology, School of Medicine, 4200 Fifth Ave, Pittsburgh, PA, USA
[b] Rothschild Foundation Hospital, 29 rue Manin, Paris, France
[c] University of Pittsburgh, Department of Bioengineering, Swanson School of Engineering, Pittsburgh, PA, USA
[d] McGowan Institute for Regenerative Medicine, University of Pittsburgh, Pittsburgh, PA, USA

ARTICLE INFO

Keywords:
AOSLO
Autofluorescence
Central serous chorioretinopathy
OCT

ABSTRACT

Purpose: To test the hypothesis that hyperreflective foci in central serous chorioretinopathy (CSCR) are autofluorescent and may represent macrophages that have engulfed outer retinal fluorophores from the retinal pigment epithelium (RPE) and photoreceptors.

Methods: Enrolled subjects underwent spectral domain and swept-source optical coherence tomography, adaptive optics flood-illumination, and adaptive optics scanning laser ophthalmoscopy (AOSLO), including near-infrared autofluorescence (AO-IRAF). For the AO-IRAF imaging, retinal fluorophores were excited using 795 nm light and collected in an emission band from 814 to 850 nm.

Results: In 2 of 3 eyes, a hyperautofluorescent signal was detected with an elliptical shape and punctate, granular aspects surrounded by a hypoautofluorescent halo. The size of these structures in the active case was measured to be 17 ± 4 μm in diameter, with at least 45 individual hyperautofluorescent foci identified from the AO-IRAF montage in the active stage of patient 2. In the asymptomatic case there were fewer structures visible (~10) and their size was smaller (11 ± 4 μm). These hyper-AF foci were colocalized with hyperreflective foci on OCT and visible in simultaneously acquired confocal AOSLO images in active stage. The hyperautofluorescent foci in the patient with active CSCR disappeared coincident with clinical resolution.

Conclusion and importance: We show here the first AO-IRAF images from patients with CSCR, demonstrating hyper-autofluorescent punctate foci, colocalized with hyper-reflective foci on confocal AOSLO images and in OCT. The autofluorescence of these foci may be driven by the accumulation of photoreceptor and RPE fluorophores within macrophages during the active stage of the disease.

1. Introduction

Central serous chorioretinopathy (CSCR) typically affects males between 20 and 50 years old. Neurosensory retinal detachment involving the macular region occurs due to leakage from the choroid through the retinal pigment epithelium (RPE).[1] CSCR pathogenesis is not fully understood, however, it is believed that choroidal abnormalities are the primary underlying pathophysiology. Subretinal fluid (SRF) in CSCR can sometimes resolve spontaneously[2,3] if diagnosed cases, however, this can lead to atrophy of the retina or RPE and potentially choroidal neovascularization. The most utilized treatment for CSCR is currently photodynamic therapy (PDT) with about 15–30% of patients having recurrence.[4,5]

The diagnosis and workup of CSCR typically involves multi-modal imaging. Structural imaging with optical coherence tomography (OCT) and scanning laser ophthalmoscopy (SLO) can quickly reveal and quantify features such as SRF. More subtle fluid-leakage can be detected with fluorescein angiography (FA). Fundus autofluorescence (FAF) can reveal additional information about the health of the RPE and the regions of interest are often described as hypofluorescent (minimal or absence of signal) or hyperfluorescent (strong signal). The RPE contains lipofuscin, and melanin that can be excited using different wavelengths of light and imaged using the red-shifted emission spectra. FAF has been used extensively to evaluate RPE status in CSCR.[6–8] However, FAF

* Corresponding author. Laboratory of Biophysics, Institute of Biomedicine University of Turku Tykistönkatu 6A, Turku, Finland.
E-mail address: kvvien@utu.fi (K.V. Vienola).

https://doi.org/10.1016/j.ajoc.2022.101741
Received 17 August 2022; Received in revised form 12 October 2022; Accepted 22 October 2022
Available online 31 October 2022

Table 1
OCT imaging parameters.

Parameter		Patient 1	Patient 2	Patient 3	
				Active	Resolved
Size X	[pixel]	384	1024	384	
	[mm]	5.9	5.6	4.4	
Size Z	[pixel]	496	496	496	
	[mm]	1.9	1.9	1.9	
Scaling X [μm/pixel]		5.78	5.49	11.40	
Scaling Z [μm/pixel]		3.87			
ART Mode (averaged)		ON (10)	ON (16)	ON (10)	ON (16)
Quality [dB]		27	20	27	18
EDI Mode		OFF	ON	OFF	
# of B-Scans		25	37	25	37
Pattern Size	[°]	20 × 20	20 × 15	20 × 20	15 × 15
	[mm]	5.9 × 5.9	5.6 × 4.2	5.9 × 5.9	4.4 × 4.4
B-scan sampling [μm]		247	117	122	

performed on conventional clinical devices lacks the resolution needed to image CSCR at a cellular level *in vivo*.[9,10]

Cellular level imaging of the living retina can be achieved with adaptive optics ophthalmoscopy (AOO).[11] AOO utilizes an adaptive optics sub-system to correct for ocular aberrations and can achieve near diffraction-limited images of the living retina.[11] Adaptive optics scanning laser ophthalmoscopy (AOSLO) produces *en face* images of the retina over a small field-of-view (FOV), typically around 1–2°[12] with a resolution of few microns that can be stitched together to form larger montages of the retina. AOSLO can implement all the same modalities as SLO including confocal reflectance and autofluorescence but with microscopic details, including individual photoreceptor and RPE cells due to the improved lateral resolution.[13,14]

OCT demonstrates hyper-reflective foci in CSCR that are considered to be accumulated shed photoreceptors foot plates, secondary to RPE dysfunction.[15] Also, there are hyper-reflective structures in the outer plexiform and outer nuclear layers and around the elongated outer segments of the photoreceptors in CSCR.[16] Recently, Iacono et al. showed that the hyper-reflective foci seen in spectral-domain OCT (SD-OCT) are colocalized with the hyperautofluorescent areas seen in the granular AF phase of the disease using Spectralis.[17] However, these images obtained using commercial devices lacked the resolution to evaluate the fluorescence signal from individual cells.[9]

Hyperreflective clusters on cross-sectional OCT in the outer retina of central serous chorioretinopathy have been imaged using AOSLO reflectance with both confocal and split-detection imaging techniques. These investigations identified three distinct patterns of these clusters and showed that they have a regular granular morphometry[18] and that they colocalize with the hyper-reflective foci previously described in SD-OCT. Those OCT hyperreflective dots are associated with longer persistence of the subretinal fluid,[19] poorer best-corrected visual acuity (BCVA), and the need for treatment in CSCR.[20] These OCT hyper-reflective clusters have been hypothesized to be either proteins, lipids, macrophages, aggregates, or retinal pigmented epithelial cells.[20]

The aim of this study was to use clinical multi-modal imaging in combination with AOSLO reflectance and autofluorescence to investigate the cellular origin of the hyperreflective foci seen in clinical structural images. We evaluated the microscopic autofluorescence of the hyper-reflective foci by using AO-IRAF. We hypothesized that these hyper-reflective foci could be hyper-autofluorescent on AO-IRAF due to the presence of fluorophores such as lipofuscin and melanin that can constrain the hypotheses regarding their cellular origin.

2. Methods

This observational study was carried out in accordance with the Declaration of Helsinki and all procedures were approved by the Institutional Review Board of the University of Pittsburgh. Informed consent was obtained from each volunteer after the risks and benefits of participation were explained both verbally and in writing. To ensure safe imaging, all light levels were kept below the American National Standard Institute (ANSI) laser safety limits and were calculated in accordance with best practices for multi-wavelength ophthalmic imaging.[21]

Table 2
Patient characteristics at the time of imaging.

Patient		Eye	VA	CMT (μm)	Description
1	49 M	OD	20/25	253	Chronic SRF in superonasal macula
2	53 F	OS	20/20	227	Resolved SRF after period of chronicity
3	56 M	OS	20/25	232	Resolved SRF after ICGA-guided half-fluence PDT 2 months prior

M/F: male/female, VA: visual acuity, CMT: central macular thickness, SRF: subretinal fluid, ICGA: Indocyanine green angiography, PDT: photodynamic therapy, OD/OS: right/left eye.

Three patients with chronic CSCR were included. Only one eye per patient was studied. Each patient underwent a complete ophthalmic examination that included the measurement of BCVA, a slit-lamp examination, and a fundus examination. Chronic CSCR was defined by persistence of subretinal fluid for more than 4 months, in association with RPE alterations as seen on FAF.

Patients underwent clinical multi-modal imaging with SLO and SD-OCT (Spectralis HRA + OCT, Heidelberg Engineering GmbH, Heidelberg, Germany); relevant scan parameters are presented in Table 1. SLO reflectance images as well as infrared autofluorescence (IRAF) and blue autofluorescence (BAF) images were acquired.

AOO was carried out using both a flood-illumination adaptive optics (FIAO) fundus camera (rtx1-e, Imagine Eyes, Orsay, France) and a research-grade custom-built fluorescence AOSLO that has been described in detail previously.[22] For AOSLO, the confocal reflectance and AO-IRAF channels were used to simultaneously acquire several image sequences of 90-s each across a 1.5° × 1.5° field of view at a frame rate of 30 Hz. A 795 nm centered (16 nm FWHM) super luminescent diode (MS-795-GI15, Superlum, Dublin, Ireland) provided confocal illumination and fluorescence excitation while AO-IRAF emission was collected between 814 and 851 nm using a bandpass filter (FF01-832/37, Semrock, USA) in the AF detection channel. Wavefront sensing was carried out using a 909 nm laser diode.

Each 90-s confocal AOSLO video (consisting of 2700 individual images) was desinusoided and registered using strip-wise registration software developed in-house.[23] AO-IRAF images were co-registered to the confocal image and averaged to increase the signal-to-noise ratio (SNR). The averaged AO images were montaged together using Adobe Photoshop (2019, Adobe Systems, Inc., San Jose, CA, USA). The brightness and contrast of individual AO images were manually adjusted to approximately balance these values across the montage.

As a final step, AOSLO and FIAO montages were manually co-registered with clinical images, using vessels and other prominent structural features as landmarks. All modalities were re-scaled to match the scale of the AOSLO images, allowing structures to be compared across modalities. Co-registered Spectralis SLO images were used to determine the precise location of SD-OCT cross sections with respect to the *en face* modalities.

To quantify the number and size of the hyperautofluorescent foci in the AO-IRAF images, ImageJ was used. A signal intensity profile was plotted (both horizontal and vertical) to which a standard Gaussian function was fitted to obtain the full-width half maximum (FWHM) of the foci.

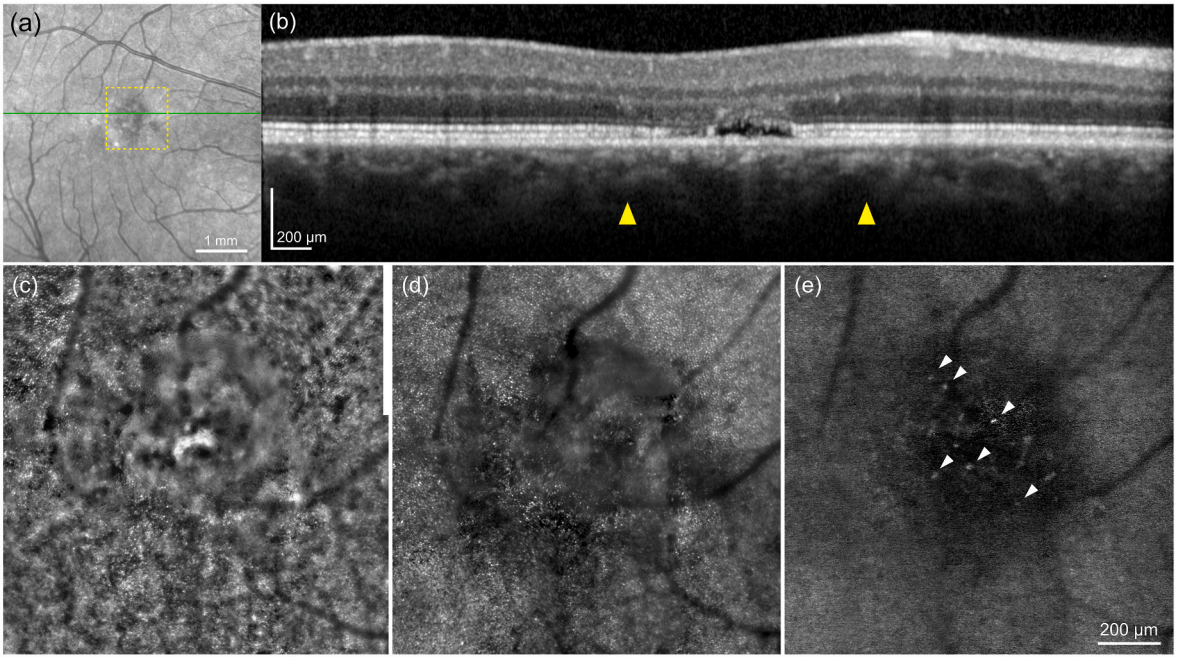

Fig. 1. Multimodal imaging of patient 1. (a) Near-infrared reflectance SLO. Dashed yellow square indicates location of AO imaging; green line localizes the OCT cross-section. (b) OCT section through chronic SRF; yellow arrowheads localizing the AO images. (c) 850 nm flood-illumination AO (d) AOSLO reflectance montage (e) AO-IRAF showing centrally-attenuated autofluorescence signal with discrete hyper-autofluorescent foci (white arrowheads). (For interpretation of the references to colour in this figure legend, the reader is referred to the Web version of this article.)

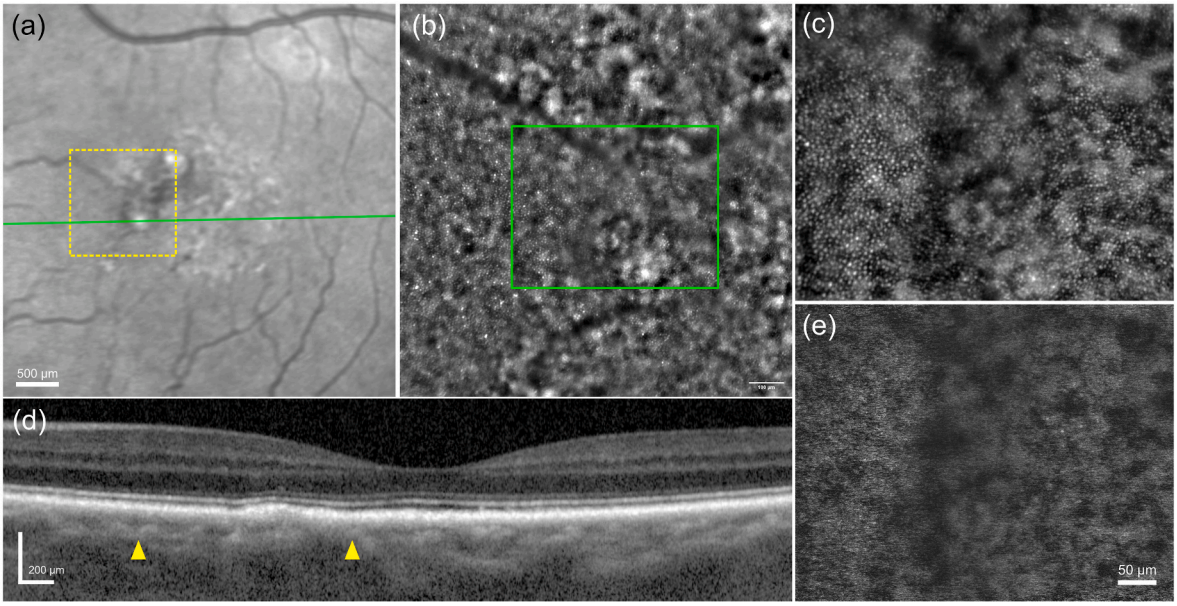

Fig. 2. Patient 2 after spontaneous resolution of SRF. (a) Near-infrared reflectance. Yellow square indicates location of FIAO imaging; green line localizes OCT cross-section. (b) Flood-illumination AO. Green rectangle localizes AOSLO images. (c) AOSLO reflectance image. (d) OCT section. Yellow arrowheads indicate boundaries of the flood AO image. (e) AO-IRAF image showing no signs of hyper-autofluorescent foci. (For interpretation of the references to colour in this figure legend, the reader is referred to the Web version of this article.)

3. Results

Patient characteristics at the time of imaging are summarized in Table 2.

Fig. 1 shows the imaging findings in patient 1. Near-infrared reflectance showed a granular alteration in reflectivity in the area of chronic SRF. The OCT cross-section showed a small pocket of SRF with disruption of the architecture of the outer retinal bands, including loss of external limiting membrane, ellipsoid and interdigitation zones. A small focus of RPE hypertransmission was also detected.

In FIAO and confocal AOSLO images (Fig. 1c and d), the photoreceptor mosaic was seen in the periphery of the field of view, but was not visible in the area of SRF, giving way to patchy signal with ill-defined boundaries. On AO-IRAF (Fig. 1e), the autofluorescent signal was attenuated in the area of SRF but, within this area, multiple hyper-AF foci were seen (white arrowheads). Approximately 13 foci emitted

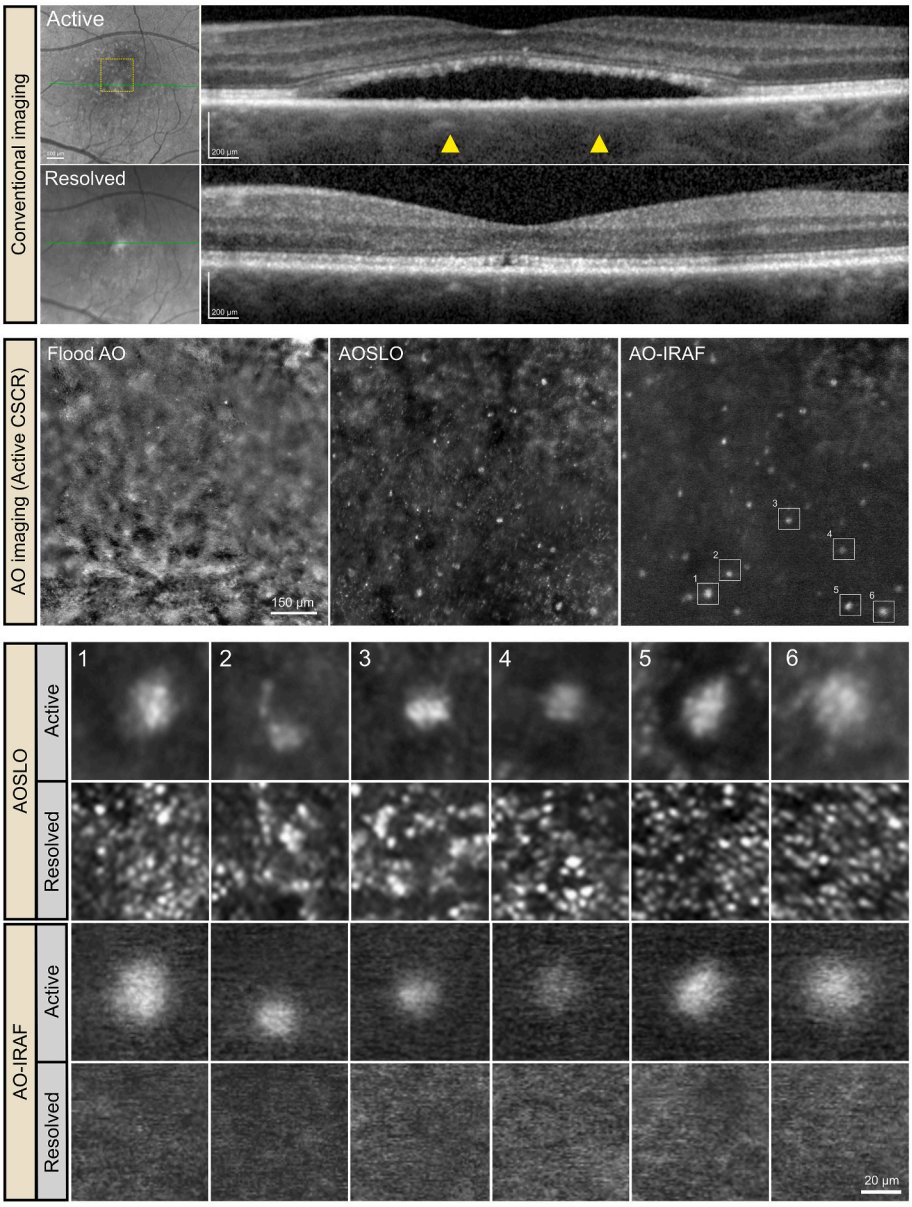

Fig. 3. Patient 3 with recurrent CSCR. Cropped images from SLO are shown for active and resolved cases on the top left corner with yellow dashed rectangle indicating AO imaging location and green line localizing the OCT scan shown on the right-hand side of the images. The AO images from the yellow dashed rectangle are shown next in the middle for the active CSCR, followed by panels, where zoomed in areas are shown from the white squares in the AO-IRAF image. (For interpretation of the references to colour in this figure legend, the reader is referred to the Web version of this article.)

sufficient autofluorescence signal to be considered above the noise floor. The mean FWHM was 11 ± 4 µm.

Fig. 2 illustrates findings in patient 2. A small, shallow, RPE elevation remained persistent without any SRF. The slightly hyper-reflective zone in the FIAO image corresponds to this RPE elevation. However, it is less prominent in the reflectance AOSLO image. The AO-IRAF shows no clear signs of hyper- or hypo-autofluorescence.

Fig. 3 shows the multimodal imaging of patient 3 with recurrent CSCR. Near-infrared fundus autofluorescence performed on the commercial SLO showed multiple central heterogeneous hyper-autofluorescent foci (not shown in Fig. 3). AO-IRAF revealed approximately 45 hyper-autofluorescent granular foci localized in the outer retina, regularly spaced from one another. The FWHM of these foci was measured to be 17 ± 4 µm, with an average hyperautofluorescent area of approximately 350 µm.[2] These AF foci co-localized with the hyperreflective foci in the AOSLO reflectance image. The area without fluid in the superonasal part of the macula did not show any specific pattern. The FIAO image showed multiple hyperreflective foci in the posterior pole but no more granular pattern either in the fundus or AO-IRAF.

4. Discussion

In this study, we used AOO including AO-IRAF to study the OCT-hyperreflective foci of CSCR, previously studied by AOSLO reflectance,[16] to test the hypotheses that these foci are hyperautofluorescent. We reproduced previously reported findings that these foci appear as granular clusters on AOSLO reflectance,[16] and we noted their presence only in eyes with SRF, and only in areas of SRF.

In eyes with active CSCR, the hyperreflective granular clusters were also hyperautofluorescent on AO-IRAF. They were not detectable by AO-IRAF, however, in eyes or regions without SRF, specifically patient 2 with inactive CSCR and patient 3 with resolved SRF after PDT. This could be attributed either to the absence of the autofluorescence sources due to structural changes accompanying the resolution of SRF or to the absence in these regions of a focal plane between the strong signal from the RPE and the discrete one from the outer retina. It is also possible that due to significant SRF, and the fact that the excitation beam is focused using photoreceptors as a guide, there is more uncertainty where the focal plane is situated, which alters our ability to acquire the AF signal. In patient 2 with inactive CSCR, the visualization of the photoreceptor

mosaic in the AO-IRAF image may have been due to the waveguiding properties of photoreceptors imposing the photoreceptor mosaic structure on the RPE AF signal. We believe this to be the case because i) photoreceptors are not known to be autofluorescent in healthy subjects, ii) we have observed this phenomenon in previous experiments, and iii) it has also been described by other groups.[22,24]

The design of this study did not enable us to conclude the cell type accounting for the AO-IRAF signal, nor did the lateral resolution of our instrument allow us to determine its intracellular origins. However, these findings should constrain future hypotheses on the cellular origin of the IRAF signal. Other limitations of the present study include the small sample size, lack of previous treatment history, and lack of follow-up on the SRF case (shown in Fig. 1). These shortcomings will be addressed in future study of a larger sample size using the "healthy" fellow eye as control.

Macrophages can originate from the activation of retinal microglia or by infiltration of monocytes into the retina from the retinal vessels, or choroid, and migrate into the subretinal space in several retinal disorders such as age-related macular degeneration (AMD), retinal detachment, and diabetic retinopathy.[25,26] Microglial activation induces local proliferation, migration, secretion of cytokines, chemokines and neurotoxins, and enhanced phagocytosis. In a study of photoreceptor clearance by microglia, Hisatomi et al. defined two types of infiltrating cells in the subretinal space: a cell of c. 10 μm diameter with lysosomes and finger-like processes, and a cell of c. 15 μm diameter containing melanin granules.[27] It is therefore possible that the IRAF emitting structures seen in chronic CSCR represent activated microglia on infiltrating monocytes involved in the phagocytosis of photoreceptor outer segments.

Retinal pigmented epithelial cells are also the primary source of autofluorescence in the retina, including melanin that resides mainly in the apical processes of the cell.[28] When injected into the vitreous under experimental conditions, RPE cells seem to undergo phenotypic and behavioral transformation and adopt macrophage-like characteristics. Phenotypic transformation is also observed in degenerative disease of the macula and neurosensory detachments. Given that melanin is a likely source for the AOSLO IRAF findings in this study, it is also possible that the OCT-hyperreflective foci under study might be transformed migratory RPE cells playing a role in phagocytosing photoreceptor outer segments shed by detached retina.

5. Conclusion

This paper presents, to our knowledge, the first AO-IRAF images of the hyperreflective foci commonly seen by OCT in CSCR. These hyperreflective foci were hyper-autofluorescent only in eyes with SRF and only in the areas of SRF. While we cannot yet conclude the cellular basis for this IRAF signal, candidate cells could include resident macrophages or RPE cells with a modified phenotype, providing the basis for subsequent experiments and further investigation. Additional studies involving donated eyes are necessary to confirm the presence of photoreceptor fragments in macrophages.

Patient consent

Written consent was obtained from all subjects to publish AO and clinical images. The report does not contain any personal information that could lead to the identification of the patient.

Funding

This research was supported by departmental startup funds from the University of Pittsburgh to ER. This work was also supported by the NIH CORE Grant P30 EY08098 to the University of Pittsburgh, Department of Ophthalmology, the Eye and Ear Foundation of Pittsburgh, NVIDIA GPU Grant Program and from an unrestricted grant from Research to Prevent Blindness, New York, NY, USA.

Authorship

All authors attest that they meet the current ICMJI criteria for Authorship.

Declaration of competing interest

The authors declare that they have no known competing financial interests or personal relationships that could have appeared to influence the work reported in this paper.

Acknowledgments

The authors would like to thank Austin Roorda for sharing their AOSLO software, Pavan Tiruveedhula for electronics fabrication and software guidance and support, Andrew Holmes for manufacturing custom mechanical components, and finally Jie Zhang, for sharing his original AOSLO optical design.

References

1. Daruich A, Matet A, Dirani A, et al. Central serous chorioretinopathy: recent findings and new physiopathology hypothesis. *Prog Retin Eye Res*. 2015;48:82–118. https://doi.org/10.1016/j.preteyeres.2015.05.003.
2. Gilbert CM, Owens SL, Smith PD, Fine SL. Long-term follow-up of central serous chorioretinopathy. *Br J Ophthalmol*. 1984;68(11):815–820. https://doi.org/10.1136/bjo.68.11.815.
3. Yannuzzi LA. Central serous chorioretinopathy: a personal perspective. *Am J Ophthalmol*. 2010;149(3):361–363. https://doi.org/10.1016/j.ajo.2009.11.017.
4. Sartini F, Figus M, Nardi M, Casini G, Posarelli C. Non-resolving, recurrent and chronic central serous chorioretinopathy: available treatment options. *Eye*. 2019;33(7):1035–1043. https://doi.org/10.1038/s41433-019-0381-7.
5. Kitzmann AS, Pulido JS, Diehl NN, Hodge DO, Burke JP. The incidence of central serous chorioretinopathy in Olmsted County, Minnesota, 1980-2002. *Ophthalmology*. 2008;115(1):169–173. https://doi.org/10.1016/j.ophtha.2007.02.032.
6. Spaide R. Autofluorescence from the outer retina and subretinal space: hypothesis and review. *Retina*. 2008;28(1):5–35. https://doi.org/10.1097/IAE.0b013e318158eca4.
7. Matsumoto H, Kishi S, Sato T, Mukai R. Fundus autofluorescence of elongated photoreceptor outer segments in central serous chorioretinopathy. *Am J Ophthalmol*. 2011;151(4):617–623. https://doi.org/10.1016/j.ajo.2010.09.031.
8. Soga H, Asaoka R, Kadonosono K, et al. Association of near-infrared and Short-wavelength Autofluorescence with the retinal Sensitivity in eyes with resolved central serous chorioretinopathy. *Invest Ophthalmol Vis Sci*. 2021;62(3):36. https://doi.org/10.1167/iovs.62.3.36.
9. Han J, Cho NS, Kim K, et al. Fundus autofluorescence patterns in central serous chorioretinopathy. *Retina*. 2020;40(7):1387–1394. https://doi.org/10.1097/IAE.0000000000002580.
10. Zola M, Chatziralli I, Menon D, Schwartz R, Hykin P, Sivaprasad S. Evolution of fundus autofluorescence patterns over time in patients with chronic central serous chorioretinopathy. *Acta Ophthalmol*. 2018;96(7):e835–e839. https://doi.org/10.1111/aos.13742.
11. Roorda A, Duncan JL. Adaptive optics ophthalmoscopy. *Annu Rev Vis Sci*. 2015;1:19–50. https://doi.org/10.1146/annurev-vision-082114-035357.
12. Roorda A, Romero-Borja F, Donnelly III WJ, Queener H, Hebert TJ, Campbell MCW. Adaptive optics scanning laser ophthalmoscopy. *Opt Express*. 2002;10(9):405–412. https://doi.org/10.1364/OE.10.000405.
13. Rossi EA, Rangel-Fonseca P, Parkins K, et al. In vivo imaging of retinal pigment epithelium cells in age related macular degeneration. *Biomed Opt Express*. 2013;4(11):2527–2539. https://doi.org/10.1364/BOE.4.002527.
14. Morgan JIW, Dubra A, Wolfe R, Merigan WH, Williams DR. Vivo autofluorescence imaging of the human and Macaque retinal pigment epithelial cell mosaic. *Invest Ophthalmol Vis Sci*. 2009;50(3):1350–1359. https://doi.org/10.1167/iovs.08-2618.
15. Cheung CMG, Lee WK, Koizumi H, Dansingani K, Lai TYY, Freund KB. Pachychoroid disease. *Eye*. 2019;33(1):14–33. https://doi.org/10.1038/s41433-018-0158-4.
16. Vogel RN, Langlo CS, Scoles D, Carroll J, Weinberg DV, Kim JE. High-resolution imaging of intraretinal structures in active and resolved central serous chorioretinopathy. *Invest Ophthalmol Vis Sci*. 2017;58(1):42–49. https://doi.org/10.1167/iovs.16-20351.
17. Iacono P, Battaglia PM, Papayannis A, La Spina C, Varano M, Bandello F. Acute central serous chorioretinopathy: a correlation study between fundus autofluorescence and spectral-domain OCT. *Graefe's Arch Clin Exp Ophthalmol*. 2015;253(11):1889–1897. https://doi.org/10.1007/s00417-014-2899-5.
18. Kon Y, Iida T, Maruko I, Saito M. The optical coherence tomography-ophthalmoscope for examination of central serous chorioretinopathy with precipitates. *Retina*. 2008;28(6):864–869. https://doi.org/10.1097/IAE.0b013e3181669795.

19. Suwal B, Khadka D, Shrestha A, Shrestha S, Shrestha N, Khatri B. Baseline predictive factors of visual outcome and persistence of subretinal fluid based on morphologic changes in spectral domain optical coherence tomography in patients with idiopathic central serous chorioretinopathy. *Clin Ophthalmol*. 2019;13:2439–2444. https://doi.org/10.2147/OPTH.S233273.
20. Lai WY, Tseng CL, Wu TT, Lin HS, Sheu SJ. Correlation between baseline retinal microstructures in spectral-domain optic coherence tomography and need for early intervention in central serous chorioretinopathy. *BMJ Open Ophthalmology*. 2017;2 (1), e000054. https://doi.org/10.1136/bmjophth-2016-000054.
21. American National Standards Institute Inc. *American National Standard for Safe Use of Lasers*. Laser Institute of America; 2014.
22. Vienola KV, Zhang M, Snyder VC, Sahel JA, Dansingani KK, Rossi EA. Microstructure of the retinal pigment epithelium near-infrared autofluorescence in healthy young eyes and in patients with AMD. *Sci Rep*. 2020;10(1):9561. https://doi.org/10.1038/s41598-020-66581-x.
23. Zhang M, Gofas-Salas E, Leonard BT, et al. Strip-based digital image registration for distortion minimization and robust eye motion measurement from scanned ophthalmic imaging systems. *Biomed Opt Express*. 2021;12(4):2353–2372. https://doi.org/10.1364/BOE.418070.
24. Grieve K, Gofas-Salas E, Ferguson RD, Sahel JA, Paques M, Rossi EA. In vivo near-infrared autofluorescence imaging of retinal pigment epithelial cells with 757 nm excitation. *Biomed Opt Express*. 2018;9(12):5946–5961. https://doi.org/10.1364/BOE.9.005946.
25. Guillonneau X, Eandi CM, Paques M, Sahel JA, Sapieha P, Sennlaub F. On phagocytes and macular degeneration. *Prog Retin Eye Res*. 2017;61:98–128. https://doi.org/10.1016/j.preteyeres.2017.06.002.
26. Silverman SM, Wong WT. Microglia in the retina: roles in development, maturity, and disease. *Ann Rev Vision Sci*. 2018;4(1):45–77. https://doi.org/10.1146/annurev-vision-091517-034425.
27. Hisatomi T, Sakamoto T, Sonoda Khei, et al. Clearance of apoptotic photoreceptors. *Am J Pathol*. 2003;162(6):1869–1879. https://doi.org/10.1016/s0002-9440(10)64321-0.
28. Bermond K, Wobbe C, Tarau IS, et al. Autofluorescent granules of the human retinal pigment epithelium: phenotypes, intracellular distribution, and age-related topography. *Investig Ophthalmol Vis Sci*. 2020;61(5):35. https://doi.org/10.1167/iovs.61.5.35.